Journal of Engineering Research and Reports

23(7): 1-15, 2022; Article no.JERR.91935
ISSN: 2582-2926

Simulation and Construction of a High Frequency Transformer-Based Inverter for Photovoltaic System Applications

Samson Dauda Yusuf [a*], Abdulmumini Zubairu Loko [a], Aminu Alhaji Abdulhamid [b] and Olorunshola Sunday Stephen [a]

[a] Department of Physics, Faculty of Natural and Applied Sciences, Nasarawa State University, Keffi, Nigeria.
[b] Department of Engineering, School of Science, Isa Mustapha Agwai Polytechnic Lafia, Nasarawa State, Nigeria.

Authors' contributions

This work was carried out in collaboration among all authors. All authors contributed to the study conception and design. Material preparation, data collection and analysis were performed by authors SDY, AZL, AAA and OSS. The first draft of the manuscript was written by author AAA, reviewed and re-drafted by author SDY, and all authors commented on previous versions of the manuscript. All authors read and approved the final manuscript.

Article Information

DOI: 10.9734/JERR/2022/v23i717619

Open Peer Review History:
This journal follows the Advanced Open Peer Review policy. Identity of the Reviewers, Editor(s) and additional Reviewers, peer review comments, different versions of the manuscript, comments of the editors, etc are available here: https://www.sdiarticle5.com/review-history/91935

Original Research Article

Received 15 July 2022
Accepted 20 September 2022
Published 06 October 2022

ABSTRACT

Aims: To simulate and construct a single phase, pure sine wave inverter using a high frequency transformer.
Study Design: Experimental design through simulation studies using pulse width modulation and proportional integral controller.
Place and Duration of Study: Department of Physics, Nasarawa State University Keffi, Nigeria, between July 2021 and March 2022.
Methodology: Secondary data from Shenzhen EMPTEK EP1100 PRO manufacturer's datasheets website was utilized for modelling and simulation of the inverter schematic using PSIM version 12.0.3 software. The system consists of DC source-Link, DC-DC converter, VS full bridge with MOSFET driver, LCL filter, HF transformer, and PI controller. The circuit was constructed at a rated power of 1kW and analysis of the inverter output was carried out over a range of steady state loading conditions.

**Corresponding author: Email: samsonyusufu@yahoo.com;*

Results: A fairly good steady state dynamic response was obtained by the system with an output voltage range of 220V to 224V, output current range of 5.02A to 5.51A; all recorded over a range of loading conditions. The highest inverter efficiency was found to be 97.47% at a load of 0.036Ω, while the power delivered by the inverter at this load was 1049.18W. The lowest value of the efficiency, which was 91.79%, occurred at the lowest load of 0.029Ω, and the output power delivered by the inverter at this load was 1172.53W.
Conclusion: The circuit combines the advantage of galvanic isolation and high conversion efficiency which reduces harmonic disturbance resulting from non-linear circuit behavior. The disadvantage of weaker load capacity and impact resistance is greatly improved using the PI controller. It can serve as a good source of alternative power supply for domestic and commercial users especially in Nigeria where the power supply is unstable and unreliable.

Keywords: High frequency; transformer based inverter; PV system; power simulation: construction; proportional integral controller; DC to AC conversion.

1. INTRODUCTION

The world demand for electrical energy is constantly increasing, especially in Nigeria where the electricity supply is epileptic [1]. Conventional energy resources are increasingly becoming unpopular, and even gradually depleting. Renewable or green energy is therefore being developed at high speed, especially solar energy [2]. One of the methods for harvesting solar energy is using the photovoltaic (PV) modules. In comparison to other kinds of renewable energy systems, there is no moving part in a solar system, which means that, the solar systems may last for a long time with minimum maintenance [3]. The general configuration of stand-alone solar PV power system comprises of PV panels array to collect/harvest the solar energy and convert it to electricity, a charge controller as a control unit, a battery as a storage device for backup at night time or cloudy weather, an inverter that converts the DC to AC, and AC loads (i.e. household appliances, lamps etc.) [4]. With the increasing popularity of solar energy sources, the need for static inverters has increased substantially [5]. Power electronics provides the industries with effective methods to save energy and improve performance, where power semiconductor devices represent the heart of modern power electronics which helps to convert power from one form to another [6]. There are four basic conversion functions that can normally be implemented, this includes AC to AC, AC to DC, DC to AC and DC to DC [7]. An inverter is one of the converter families which is called DC to AC converter. It converts DC (direct current) power to AC (alternating current) power with symmetric AC output voltage at desired magnitude and frequency. It is widely used in industrial applications such as variable speed AC motor drives, induction heating, standby power supplies and uninterruptible power supplies [5]. The DC power input of inverter can be obtained from the existing power supply network, a battery source, photovoltaic source, wind energy, fuel cell or other DC sources [8].

In PV systems, inverters are used to convert DC electricity generated from a solar panel or battery to AC electricity, so as to either supply consumer households or to connect directly to the utility grid. This conversion can either be achieved by transistors or by SCRs (silicon controlled rectifiers) [9]. However, MOSFETs (Metal Oxide Semiconductor Field Effect Transistor) and IGBTs (Insulated Gate Bipolar Transistor) are good candidates for the switches in DC to AC conventional techniques [10]. For lower and medium power outputs, transistorized inverters are suitable, while for high power outputs, SCRs are employed. In a conventional inverter, transformer is used to match the inverter output with the utility grid output. However, a transformer can be bulky, very heavy and highly inductive which hampers the overall power factor correction in the inverter system [11]. Switched-mode DC-to-AC inverters are used in a wide range of applications where the objective is to produce a sinusoidal AC output whose magnitude and frequency can both be controlled. The DC voltage is obtained by rectifying and filtering the line voltage, most often by diode rectifier circuits [12].

Several previous studies have developed various models over the years. Hussein [13] simulated the design of a 2-stage conversion online UPS system based on a low frequency transformer. Ehikhamenle and Okeke [14] developed a 2.5kVA low frequency inverter using a Microcontroller Based Frequency counter with a boost converter. Diouri et al. [15] proposed a

high-performance transformerless, single-phase PV inverter in the standalone mode, using a nonlinear back-stepping control. Combination of fuzzy logic and proportional resonant (PR) control to suppress leakage current in a transformerless inverter for grid-connected PV systems was proposed by Suresh et al. [16]. Muhanned [17] developed a transformerless voltage source inverter (VSI) through H-Bridge configuration and achieved the switching control using microcontroller-based PWM. Khan et al. [18] presented a comprehensive state-space dynamic model of a future power distribution system for plug-and-play interface of distributed renewable energy resources and distributed energy storage devices using multiple solid-state transformers (SSTs). Khan et al. [19] proposed a novel full-bridge inverter, using a single inductor buck-boost converter and high frequency transformer to obtain an isolated well-regulated voltage output. Patel et al. [20] developed a high frequency inverter using a HF transformer and full-bridge rectifier scheme to obtain galvanic isolation, as well as fast recovery rectification between the input and output of the inverter. Jiang et al. [21] employed a high frequency transformer in integrating a Z-source network concept into a two-stage DC-DC-AC topology.

Conventional low frequency transformer-based inverters require the use of low frequency isolation transformers to step up the converted voltage to a value suitable for low, medium and high voltage applications. However, the use of low frequency transformer involves employing the use of inductive components with heavy current-carrying capacities. This imposes additional load on the primary DC sources and consequently, affects the overall system efficiency with attendant cost implications [22]. Furthermore, the low frequency transformer-based inverters requires special arrangements for compatibility in grid-tied applications due to their circuit complexity [23]. Modern power electronic converters tend to use “more silicon and less iron.” This leads to the pursuance of compact designs with wide input voltage ranges and improved overall efficiency such as the transformerless inverters [24]. One of the main drawbacks in transformerless single phase photovoltaic inverter is to control leakage current appearing between parasitic capacitor and ground [25]. To overcome these problems, the main objective of this study is to simulate and construct a high frequency transformer inverter for PV system applications. High frequency transformers are generally employed to achieve galvanic isolation as well as higher efficiency for majority of inverter applications [26]. A high frequency transformer (HFT) designed using SST-based power delivery architecture has advantages in terms of smaller size and weight, less harmonics, power density, scalability, and owing to the use of solid state devices; reduces the on-state resistance, thereby increasing the overall efficiency of converters especially in inverter applications [27]. A solid state transformer (SST) is a power electronics-based transformer with controllable communications and remote-sensing capabilities, as well as ride-through functionalities [18]. The use of a HFT-based inverter will reduce the amount of heat generated in the system, increase the overall system efficiency and greatly reduce the system cost. The advantages of the proposed high frequency inverter over the low frequency inverter of the same power in this study is light weight, small size, small standby power, and high efficiency. Even though the circuit is relatively complex, the disadvantage of weaker load capacity and impact resistance is greatly improved using the proportional integral (PI) controller. This in turn will make the realization of a smart inverter with a relatively straightforward process and precision-prone prediction algorithms.

2. MATERIALS AND METHODS

2.1 Materials

The materials and their specification that were used for the simulation and construction of a 1.5kVA pure sine wave, high frequency inverter includes PSIM v12.0.3 Power Electronics Design Software, E65-N27 Transformer Ferrite Core, 495-5498-ND Bobbin Coil, IR2010PBF-ND IC Gate Driver, SG3525ANGOS-ND IC Regulator Control, BER169-ND Thermal Pad (Heat Sink), STP160N75F3 N-Channel MOSFET, STTH8R06 Rectifier Diodes, and Fluke 87V Digital Multimeter.

2.2 Methods

2.2.1 Simulation method

Secondary data on the designed circuit was obtained from the Shenzhen EMPTEK EP1100 PRO manufacturer’s datasheets website. This was then utilized in reconfiguring the design to suit the scope of the current study. Various stages of the circuit design were modeled and simulated using power simulation (PSIM)

software version 12.0.3 for conformity to the design criteria, as well as to consider device configuration options for optimal circuit reliability and performance. The block diagram of the proposed inverter system is shown in Fig. 1. The system consists of the DC source/DC-Link, the DC-DC converter, the VS full bridge circuit along with the MOSFET driver module, the LCL filter, the HF transformer and the PI controller.

The application environment was launched and the necessary circuit parameters and equations were defined for various parts of the system including output voltage, load current, power handling efficiency, and total harmonic distortion. These parameters were analyzed under various steady state conditions, while relevant expressions developed by Rashid [28] for the subsystem parameters were used to optimize the model characterization.

2.2.1.1 Inverter output voltage (V_{out})

The inverter Output Voltage (V_{out}) was determined from the expression:

$$V_{out} = 2\left(\frac{N_2}{N_1}\right) DV_{in} \quad (1)$$

Equation (1) was obtained from the voltage source inverter transfer function, where $\left(\frac{N_2}{N_1}\right) = N$ is the high frequency transformer turns ratio; D is the DC-DC converter duty cycle (usually specified) in the manufacturers' datasheets; and V_{in} is the inverter input voltage which in essence is the output from the boost stage.

2.2.1.2 Switching period (T)

The driver circuit switching period was determined using the expression as defined by Rashid [28] as:

$$T = \frac{1}{f} \quad (2)$$

Where f = the switching frequency of the inverter MOSFETs.

2.2.1.3 Maximum duty cycle (D)

The maximum combined duty cycle (D) for both half cycles in the DC-DC converter as defined by Rashid [28] was determined as follows:

$$D = \frac{0.9t_{on}}{T} \quad (3)$$

Where t_{on} is the conducting period for the positive half cycle of each bank of MOSFETs in the DC-DC converter.

2.2.1.4 Inverter input power (P_{in})

The inverter input power (P_{in}) was determined by the expression as defined by Rashid [28] as:

$$P_{in} = \frac{P_{out}}{\eta} \quad (4)$$

Where P_{out} is the inverter rated power output (usually specified), and η is the inverter conversion efficiency, which can also be determined from the expression as defined by Eichhorn [29] as follows:

$$Efficiency = \frac{P_{Out}}{P_{Out}+Losses} \quad (5)$$

2.2.1.5 Maximum average input current (I_{in})

The maximum average input current in the inverter (I_{in}) was determined from Equation (6) as defined by Rashid [28] as follows:

$$I_{in} = \frac{P_{in}}{V_{in}} \quad (6)$$

2.2.1.6 Maximum MOSFET RMS current (I_{MOS_RMS})

The maximum RMS current (I_{MOS_RMS}) for the driver circuit MOSFETs was determined using Equation (7) as defined by Rashid [28] as:

$$I_{MOS\_RMS} = I_{pft}\sqrt{D} \quad (7)$$

Where I_{pft} is the maximum equivalent flat topped input current of the inverter which have been defined by Rashid [28] as follows:

$$I_{pft} = \frac{I_{in}}{2D} \quad (8)$$

2.2.1.7 Minimum MOSFET breakdown voltage ($V_{MOS_{Breakdown}}$)

The minimum MOSFET breakdown voltage ($V_{MOS_{Breakdown}}$) was determined using the equation defined by Rashid [28] as follows:

$$V_{MOS_{Breakdown}} = 1.3 \times 2 \times V_{Converter_{MAX}} \quad (9)$$

Where ($V_{Converter_{MAX}}$) is the converter maximum allowed input voltage (usually specified in the datasheets).

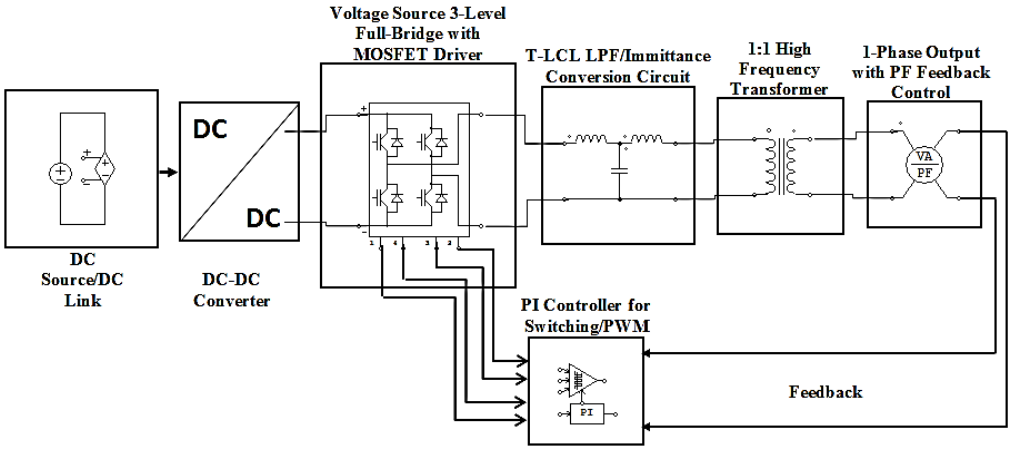

Fig. 1. Block diagram representation of the proposed inverter

2.2.1.8 Transformer turns-ratio (N)

The high frequency transformer turns-ratio ($N = \frac{N_2}{N_1}$) can be determined as suggested by Rashid [28] from the expression:

$$N = \frac{N_2}{N_1} = \frac{V_{out}}{2V_{Converter_{MIN}} \cdot D} \quad (10)$$

Where ($V_{Converter_{MIN}}$) is the converter minimum allowed input voltage also specified in datasheets.

2.2.1.9 Maximum average output current (I_{out})

The inverter maximum average output current was determined from Equation (11) defined by Rashid [28] as follows:

$$I_{out} = \frac{P_{out}}{V_{out}} \times P.F. \quad (11)$$

2.2.2 Construction method

The components were first assembled on a breadboard for small signal analysis before the actual fabrication on a printed circuit board (PCB). Various checks were carried out using digital multimeter, virtual and handheld oscilloscopes, while the components were mounted on the breadboard without soldered connections. These checks were carried out to ensure conformity with expected steady state responses and to minimize component defects during final mounting on printed circuit board. The PCB was produced following the PSIM design details. Final surface mounting was done with the boost stage, driver stage and PWM all mounted on the same board.

2.2.3 Testing method

The final prototype was assembled temporarily on a breadboard and tested for conformity with the design specifications, before final mounting on printed circuit board and encasement. DC power supply was used to provide the DC source, which was tested for both voltage and current as the output was varied from 0 to 28Vdc. Both converter and inverter outputs were measured for both on-load and off-load steady state responses. Readings were observed on digital multimeter as well as signal waveforms on handheld oscilloscope.

3. RESULTS

3.1 Data Specification

The data specifications for the DC-DC converter section, the driver/switching/modulation section and the high frequency transformer of the inverter are presented in Tables 1 to 3.

Table 1. Inverter design specifications

Specification	Value
Nominal Voltage Input	180Vdc
Output Voltage	220Vrms (±0.5%) at 50 Hz
Max Output Power (P_{out})	1.11kVA
Switching Frequency	100 kHz
Target Efficiency (η)	99%

Table 1 presents data for the inverter main parameters. The inverter nominal input voltage is the voltage sensed by the inverter driver circuit, mainly consisting of the SG3525A Pulse Width Modulator. The output voltage which is a pure

sinusoidal component with frequency 50Hz without any harmonics is measured at the filter stage and fed to the load. The maximum output power is the apparent power or the expected power handling capacity of the inverter at minimum loading (the actual power, which is rated in kilowatts, is dependent on the load current). While, the inverter switching frequency refers to the switching intervals between the 2 MOSFET banks, which is controlled by the SG3525A Pulse Width Modulator Control Circuit. Table 2 presents the DC-DC converter's main specified parameters. The nominal voltage input (V_{in}) is the voltage from the DC source (battery bank) to the converter input. The value of this voltage fluctuates between the maximum value (V_{in_max}) and minimum value (V_{in_min}) depending on the converter mode (buck mode or boost mode). The nominal output power refers to the power required to facilitate the conversion process at 99% efficiency. While, the target efficiency is the expected efficiency given the output power of the converter. Table 3 presents the transformer's main specification. The high frequency transformer nominal input voltage is the same as the output from the inverter filter circuit. The transformer switching frequency is the maximum frequency that the transformer can withstand from the inverter driver circuit. The window utilization factor (K_u) is a factor which takes into account the fact that; not all transformer core magnetic path would be fully utilized by the set up magnetic flux (both primary and secondary) linkage. This is used for derating the transformer (i.e. specifying its use for a rating slightly less than its full rated capability).

Table 2. DC-DC converter design specifications

Specification	Value
Nominal Voltage Input (V_{in})	12 V
Maximum Voltage Input ($V_{in\text{-}max}$)	28 V
Minimum Voltage Input ($V_{in\text{-}min}$)	7.5 V
Nominal Power Output (P_{out})	1.3 kW
Nominal Output Voltage (V_{out})	180 V_{dc}
Target Efficiency (η)	99.3 %
Switching Frequency (f)	30 kHz

3.2 Simulation Results

Simulation of the pure sine wave inverter was done in two stages: implementation and testing of the inverter along with the DC-DC converter, and implementation and testing of the high frequency transformer. The DC-DC converter simulation was realized using the converter wizard (Model Advisor) and the output parameters were obtained as shown in Fig. 2.

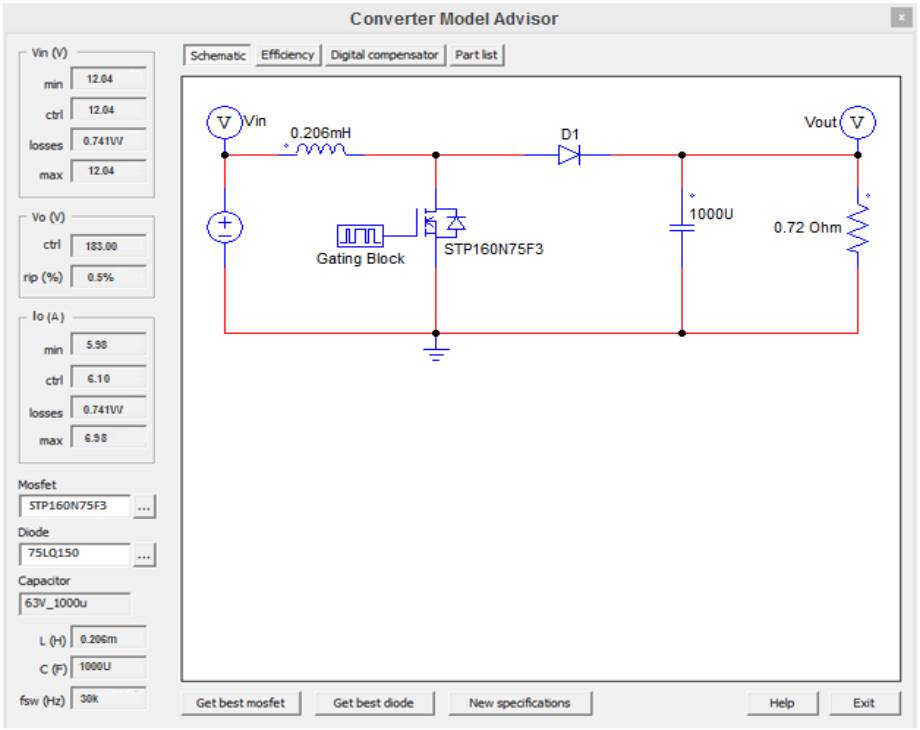

Fig. 2. Implementation of the DC-DC converter model

Table 3. High frequency transformer design specifications

Specification	Value
Nominal Voltage Input (V_{in})	220V
Switching Frequency (f)	30 kHz
Efficiency (η)	98 %
Regulation (α)	0.05 %
Maximum Operating Flux Density (B_m)	0.05 T
Window Utilization (K_u)	0.3
Temperature Rise (T_r)	30 degrees Celsius
Power Factor	0.95

The output parameters of the modeled converter is shown on the model advisor parameter windows. The simulated minimum input voltage; which is 12.04 Volts (DC) equals the simulation controlled value of the input voltage, as well as the maximum value. This is because the battery source is maintained highly stable by the PI controller; modeled by the optocoupler. The converter simulated output voltage is 183 Volts (DC) with a ripple of 0.5%. The simulated minimum output current is 5.98 Amps, whereas the simulated maximum output current is 6.98 Amps, while the simulation controller maintains the value at 6.10 Amps. The entire converter system losses are determined based on the different input/output power balances for each respective component as sensed by the PI controller (digital compensator). A comprehensive analysis of the converter system losses is illustrated in Fig. 3 alongside the percentage contribution of each component to the overall converter losses. The efficiency of the converter was then determined using equation (5). The switching frequency is maintained at 30kHz.

The inverter driver stage drain voltage was tested at approximately 205 V_{pp} and was passed through the LC filter at the output of the inverter. The schematic of the simulated inverter circuit is shown in Fig. 4. It consists of battery source, dc-link modeled by the 2 parallel capacitors, full bridge inverter section consisting of 8 MOSFET switches, load modeled by 120-ohm impedance, and PI controller modeled by the optocoupler C; which combines 2 voltage markers to be processed by the PI controller.

One voltage marker is labeled V_{ref} and is a sinusoidal signal. While, the other one is a saw tooth signal labeled V_{tri}. The 2 voltage markers are used to get the information on the inverter output voltage during every switching instant. This information is used to trace the plot of the inverter output voltage. The comparator C compares the reference and triangular (saw tooth) voltage signals in order to adjust the modulation index during pulse width modulation (PWM), which in turn, controls the driver circuit switching periods and duty cycles accordingly. The simulation steady state parameters are shown in the form of data preview dashboard in Fig. 5, while Fig. 6 shows the modeled PI controller.

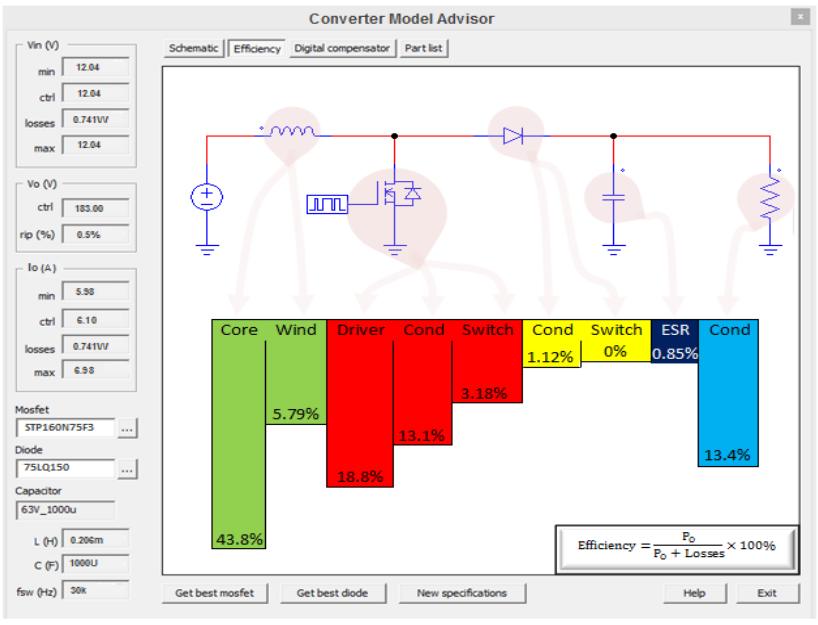

Fig. 3. DC-DC converter losses analysis and efficiency calculation

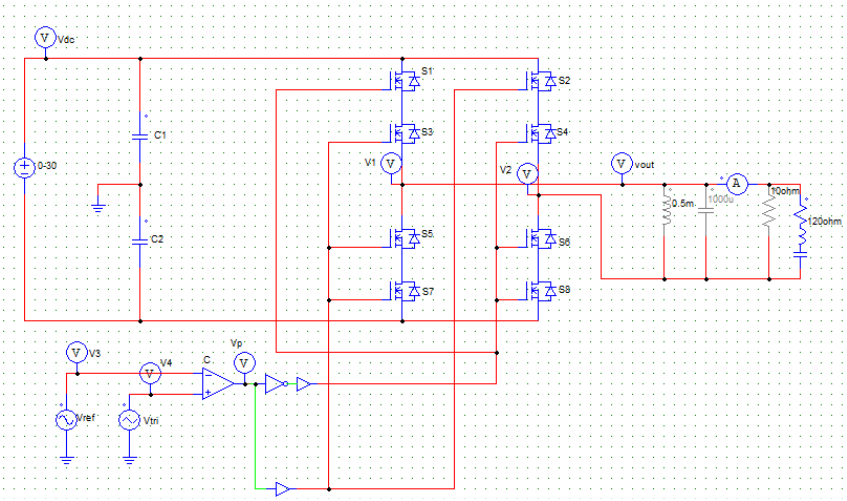

Fig. 4. Simulated inverter system

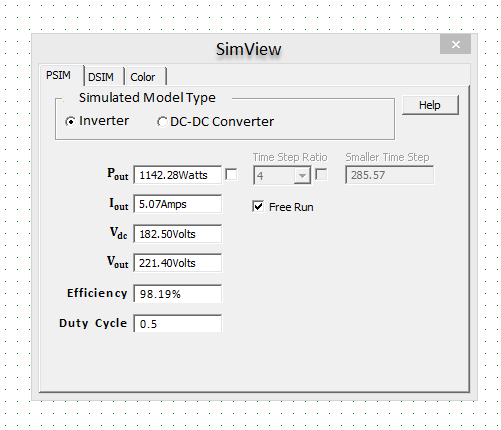

Fig. 5. Steady state parameter values

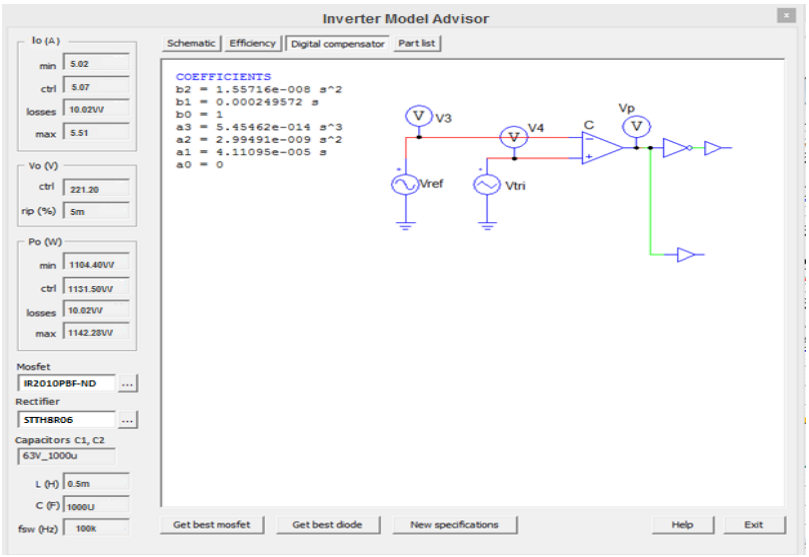

Fig. 6. Implementation of the PI controller

3.3 Circuit Construction

A prototype of the inverter was initially built on a breadboard as illustrated by the detailed circuit diagram in Fig. 7, before final transfer to a printed circuit board (Fig. 8). A suitable connector CON1 was provided on the PCB (Fig. 8(a)) to connect the MOSFET banks and the transformer externally. MOSFETs were mounted on heat-sinks using mica spacers as the insulators between them. The high frequency transformer winding on the secondary side (HV) consists of 22 bundles of 3 turns around the bobbin. Secondary side was wound first to accommodate the thick wires for the centre tap primary windings. Subsequently, the primary was wound along with centre tap wires terminated at the bobbin. In order to reduce the air gaps, a zip tie was used through the bobbin, thereby, clasping the two E-cores as much as possible. The 12V supply terminal was connected directly to the centre tap of the primary winding of the high frequency transformer, which is able to carry up to a maximum current of more than 50 amperes with 1000 Watts (±15%), although, current depends on the load applied. There is no need to add a switch in the high-current path to make the inverter turn ON and OFF. The inverter can be switched ON and OFF by low-current switch S1. The single-side PCB for the sine wave inverter circuit is shown in Fig. 8(a), while its component layout is shown in Fig. 8(b).

A proper gate driver was provided to switch at the required frequency and also maintain the duty cycle needed. The SG3525A Pulse Width Modulator Control Circuit was chosen in this study for several reasons. First, it provides a wide range of switching frequency (100 Hz to 100 kHz). Secondly, it has a built in soft-start circuitry to ensure no fast buildup charges. Thirdly, dead-time is simply arranged by connecting a single resistor between the CT and Discharge pins.

The driver was used in voltage mode control as the input voltage is not a constrained source and will vary. Voltage mode is also advantageous in applications where high power is needed; such as in this instance. Also, in practice, the leakage inductance from the high frequency transformer causes significant over-voltages across the transistor and thus; the breakdown voltage of these devices should be higher than twice the input voltage. The STP160N75F3 N-Channel Power MOSFET's were selected for the DC-DC converter design. These MOSFET's provide an ultra-low on-resistance and can handle up to 75 Volts with 120 Amps at 25°C. These switches provide extremely fast switching and can be operated normally up to 175°C. Fig. 9 shows the top view of the constructed device in a casing fabricated at Samanja Electronics Ltd, Kano using computer-aided auto-routing and differential pair routing.

3.4 Casing and Packaging

The casing is made of a BS 4607 heat-treated polyvinyl chloride (PVC) junction box; measuring 254mm x 165mm x 63mm as shown by the isometric representation in Fig. 10. The PCB is placed in the middle of the PVC casing and secured using adhesive binding compound to secure the base of the PCB and the inside bottom of the casing. The cooling fan and DC input connectors are mounted on a tapered aluminium plate, which in turn is secured to the rear-side of the casing, while providing additional cover to the opening provided for proper positioning of the DC input connectors as well as the cooling fan. The top of the casing is provided also by a heat-treated PVC material, which is secured in place by four 4½mm screws. Convenient openings located directly across the 2 heat-sinks on either sides of the casing provide heat escape and ventilation for the circuit within. External connection to the battery terminals is provided via two 10-Amp crocodile clips. An AC outlet and a power switch are provided at the front-end of the casing directly opposite the cooling fan and DC input terminals. Also, two indicator lights are provided with; one to serve as power ON indicator (colored green) and the other to serve as fault indicator (colored red). The complete packaged device on load (Table fan, mobile phone and laptop) is shown in Fig. 11.

3.5 Testing

Various tests were carried out to capture various steady state responses of the system. The components were first tested on the breadboard to avoid any imposed signals resulting from temperature changes, electromagnetic interference and unwanted readings from adjacent connections that may be energized. The DC input source was taken from a variable DC supply with a range of 0 - 35Vdc (5Amps). A variable RLC load with impedance of 0 – 120 ohms was provided. During the initial test carried out on the DC-DC buck-boost converter, the variable DC input was varied from 0 to 30 volts to determine the output of the DC-DC buck-boost converter and the results are presented in Table 4.

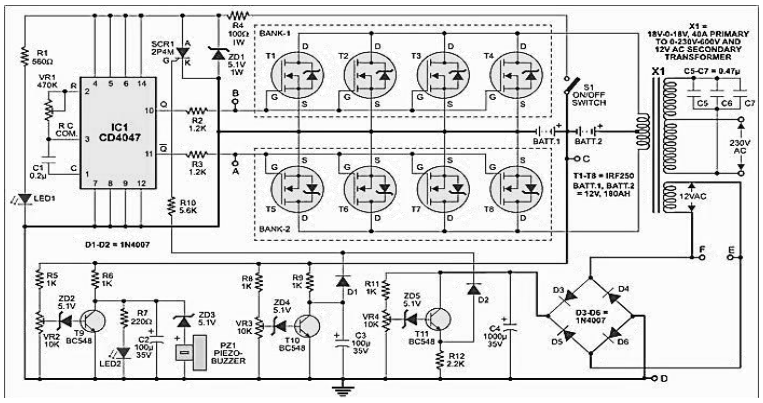

Fig. 7. Circuit wiring arrangement as mounted on Vero board

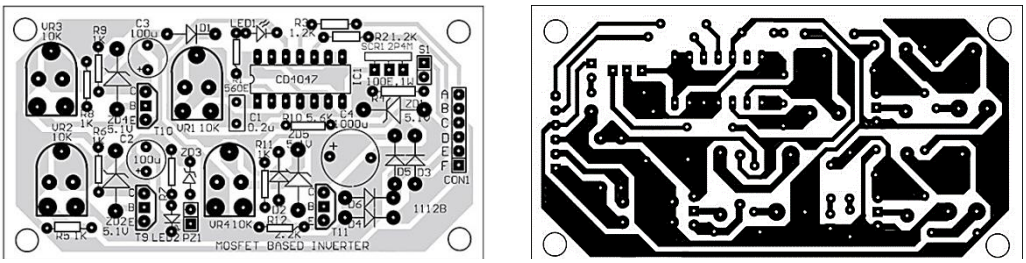

a) Component Layout on the PCB b) Single-side PCB for the sine wave inverter

Fig. 8. Component layout on the PCB and single-side PCB for the sine wave inverter circuit

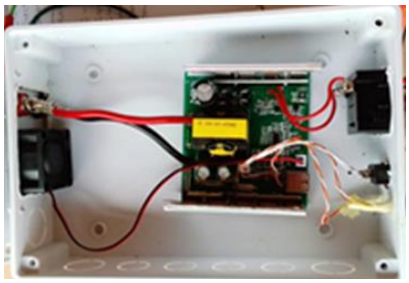

Fig. 9. Top view of constructed device in casing

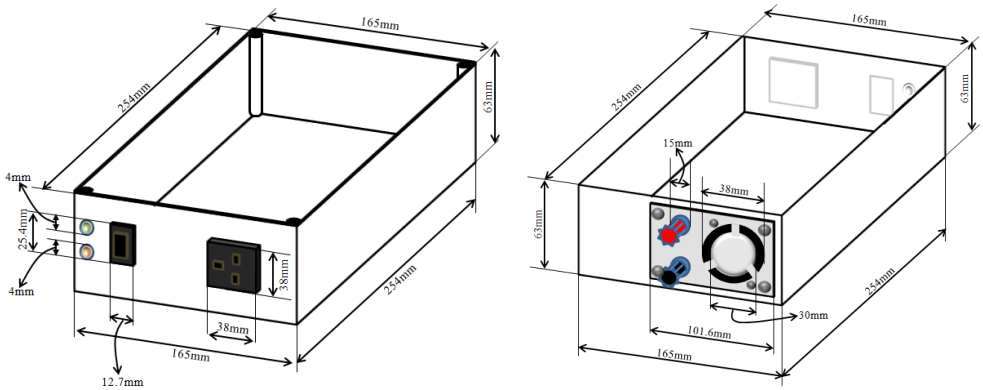

a) Front view of casing **b) Back view of casing**

Fig. 10. Isometric representation of the casing (front and back view)

Fig. 11. Constructed device on load

Table 4. Steady state DC-DC boost converter loading test results

Load (Ω)	V_{in} (V)	I_{in} (A)	V_{out} (V)	I_{out} (A)	D (%)
0.037	12.04	5.23	182.10	5.98	0.5
0.036	12.04	5.30	182.50	6.10	0.5
0.033	12.04	5. 48	183.00	6.38	0.5
0.029	12.04	5.80	183.01	6.98	0.5

Table 5. Steady state inverter loading test results

Load (Ω)	V_{in} (V)	I_{in} (A)	V_{out} (V) (No-Load)	V_{out} (V) (On-Load)	I_{out} (A)	P_{out} (W)	η (%)
0.037	182.10	5.98	230.00	220.0	5.02	1049.180	96.35%
0.036	182.50	6.10	230.00	221.20	5.07	1065.406	95.7%
0.033	183.00	6.38	230.00	223.90	5.35	1137.967	97.47%
0.029	183.01	6.98	230.00	224.0	5.51	1172.528	91.79%

Table 4 presents the result obtained during the converter steady state loading test. V_{in} is the input DC voltage from the battery source, which is maintained steady in order to determine the most accurate estimate of the output voltage, as well as help to indicate the dynamic and the steady state response of the DC-DC converter. I_{in} is the input current, which although driven by the DC input voltage, is heavily influenced by the load. V_{out} and I_{out} are the output voltage and output current respectively which serve as the inverter DC-link-fed input. D is the duty cycle, which is an influencing factor of the DC-DC converter switching ON-time (as seen from equation 3) and is usually specified in the datasheet. A final steady state loading test was conducted to observe the inverter output voltage stability over a range of loads and the result is presented in Table 5.

Table 5 presents the result obtained during the inverter steady state loading test. V_{in} is the input DC voltage, which is essentially the voltage from the DC-DC converter output, while I_{in} is the input current also from the DC-DC converter system output. V_{out} (no-load) is the output voltage recorded with the inverter system connected to No load, while V_{out} (on-load) is the recorded steady state voltage with the inverter connected to various loads. The output current I_{out} is the current output as the load is varied. P_{out} is the inverter output power which is essentially obtained using equation (11).

Thus, at the highest value of the load (0.037Ω), considering Table 5, the output power is given by:

$$\mathrm{P_{out}} = \mathrm{V_{out}} \times \mathrm{I_{out}} \times \text{Power Factor (P.F)} = 220 \times 5.02 \times 0.95 (\text{see Table 3 for P.F.})$$

$$\mathrm{P_{out}} = 1088.958 \times 0.95 = 1049.18\mathrm{W}$$

And the efficiency at this power is obtained by using equation (4) as follows:

$$Efficiency\ (\eta) = \frac{P_{out}}{P_{in}} \times 100(\%)$$

$$Efficiency\ (\eta) = \frac{1049.18}{1088.958} \times 100(\%) = 96.35\%$$

Now, at the lowest load condition (0.029Ω), considering Table 5, the output power is given by:

$$\mathrm{P_{out}} = \mathrm{V_{out}} \times \mathrm{I_{out}} \times \text{Power Factor (P.F)} = 224 \times 5.51 \times 0.95 = 1172.528\mathrm{W}$$

And the efficiency at this power is obtained by using equation (4) as follows:

$$Efficiency\ (\eta) = \frac{P_{out}}{P_{in}} \times 100(\%)$$

$$Efficiency\ (\eta) = \frac{1172.524}{1277.409} \times 100(\%) = 91.79\%$$

Note: Equation (6) is used to obtain the power input (P_{in}) to the inverter.

4. DISCUSSION

The efficiency of an inverter indicates how much DC power is converted to AC power. Sine wave inverters rated at 90% efficiency and above are ranked highly efficient, while lower quality modified sine wave inverters are considered less efficient at 75-85% rated efficiency. Some of the power is lost as heat, while some stand-by power is consumed for keeping the inverter in powered mode [30]. This ranking is adopted by the two foremost global regulatory standards for inverter efficiency; European Union Weighted Efficiency and California Energy Commission Weighted Efficiency.

High frequency inverters are usually more efficient than low-frequency variants. However, the range of values for the inverter efficiency in the current study ranges between 91.79% and 97.47%, which exceeds the global minimum average of 90%. This finding is in line with the findings of Guo et al. [31], who worked on the implementation of a single-phase six-switch current source inverter using one-dimensional space vector pulse width modulation (SVPWM) and obtained 92.8% efficiency. Also in line with that of Kerekes et al. [32] who obtained a conversion efficiency of 96% in their study on high-efficiency single-phase transformerless PV inverter topology based on the H-Bridge, with a new AC bypass circuit consisting of a diode rectifier and a switch with clamping to the DC midpoint. Also similar to the findings of Chakraborty and Razak [33] who obtained 97.1% in their work on the design of a transformerless grid-tied inverter (GTI) using dual-stage switch mode boost converter, a dual-stage switch mode buck converter, an H-bridge inverter, and a T-LCL (T-shaped inductor-capacitor-inductor low pass filter) immittance conversion circuit. On the other hand, findings of this study is not in line with the findings of Umesh et al. [34] who carried out the Design and Simulation of Single Phase Photovoltaic Inverter using Simulink; and obtained 80% conversion efficiency. The difference could be attributed to the absence of a DC-DC converter system in their design, while the current study fully exploited the advantages of DC-DC converter conditioning at the expense of simplicity. Also not in line with that of Babarinde et al. [35], who carried out the Design and Construction of 1kVA Inverter using a low frequency transformer; and obtained an efficiency of 85%. The use of low frequency transformer; even though an efficient means of providing galvanic isolation, dissipates a large amount of power as heat in the transformer core and windings, which in turn greatly reduces the efficiency of the inverter. The current study used a high frequency transformer for galvanic isolation, and hence the dissimilarity in results of the two studies.

Through the use of high frequency transformer, the current study was able to achieve an efficiency of up to 97%, while providing galvanic isolation as well as fairly good harmonic mitigation as can be seen from Table 5 where the voltage output while the inverter was loaded remained fairly constant. None of the reviewed literature achieved this as those studies with higher frequencies traded off galvanic isolation by using transformerless topologies, while other studies such as that of Babarinde et al. [35] used low frequency transformers and achieved good galvanic isolation, but traded off higher conversion efficiency.

5. CONCLUSION

An inverter converts the DC electricity from sources such as batteries or fuel cells to AC electricity. The electricity can be at any required voltage. In particular, it can operate AC equipment designed for mains operation or rectified to produce DC at any desired voltage. The input voltage, output voltage, frequency, and overall power handling depend on the design of the specific device or circuitry. The inverter does not produce any power; the power is provided by the DC source. A power inverter can be entirely electronic or may be a combination of mechanical effects (such as a rotary apparatus) and electronic circuitry. Static inverters do not use moving parts in the conversion process. Power inverters are primarily used in electrical power applications where high currents and voltages are present. This study carried out simulation of an inverter circuit designed for

single phase photovoltaic (PV) system applications. The circuit simulation was carried out using Power Electronic Simulation Software (PSIM) version 12.0.3, while the switching was provided using high-power MOSFETs and the sinewave was realized using pulse width modulation (PWM). The rated output power of the inverter was 1.0kW at 95% efficiency. A boost converter scheme was used to accomplish initial voltage conditioning in the system, while an inductor-capacitor-inductor (LCL) filter was employed for harmonic mitigation. Galvanic isolation was provided using high-frequency transformer with suitable transformation ratio. Steady state analysis was performed using only output waveforms from the simulation studies. The project met the expectations in most cases, however, in certain loads the efficiency was greater than the efficiency at both the highest and lowest loads and no particular factor was identified to which this could be attributed. The system was able to provide a regulated voltage output to an AC load at all power levels. The inverter has the advantages of light weight, small size, small standby power, and high efficiency. Even though the circuit is relatively complex, the disadvantage of weak load capacity and impact resistance is greatly improved using the proportional integral (PI) controller. As such, it can serve as a source of alternative power supply for domestic and commercial users, especially in Nigeria where the power supply is unstable, not regular in pattern, unpredictable, and better still unreliable. It is recommended among other things that active temperature protection be included for all semiconductor switches, while a suggestion for future studies is for the design and inclusion of a smart battery monitoring algorithm with overcharging and undercharging control capabilities. In addition, a better AC load regulation and protection scheme can be added, using PID control as well as Implementation of a 5-level PWM for better THD performance at the output. Also the overall efficiency of the system can be improved by using exotic converter types such as, resonant converters with synchronous rectification at the boost stage.

COMPETING INTERESTS

Authors have declared that no competing interests exist.

REFERENCES

1. Vincent EN, Yusuf SD. Integrating renewable energy and smart grid technology into the Nigerian electricity grid system. Smart Grid and Renewable Energy. 2014;5(1):220-238. DOI:http://dx.doi.org/10.4236/sgre.2014.59021.
2. Teodorescu R, Liserre M, Rodríguez P. Grid Converters for Photovoltaic and Wind Power Systems. Chichester, UK: John Wiley & Sons; 2010.
3. Blaabjerg K, Ma F, Yang Y. Power electronics - the key technology for renewable energy systems. Conference Proceedings, Ninth International Conference on Ecological Vehicles and Renewable Energies (EVER). 2014;1–11. DOI:10.1109/EVER.2014.6844159.
4. Ali W, Farooq H, Rehman A, Awais Q, Jamil M, Noman A. Design considerations of stand-alone solar photovoltaic systems. 2018 International Conference on Computing, Electronic and Electrical Engineering (ICE Cube), Quetta, Pakistan; 2018. DOI:10.1109/ICECUBE.2018.8610970.
5. Agarwal A, Marlino L, Ivester R, Johnson M. Wide bandgap power devices and applications; the U.S. Initiative. 46th European Conference on Solid-State Device Researches, Cracow, Poland. 2016;206–209. DOI:10.1109/ESSDERC.2016.7599622.
6. Elasser A, Chow TP. Silicon carbide benefits and advantages for power electronics circuits and systems. Proceedings of the IEEE, Torino, Italy. 2002;90(6):969–986. DOI:10.1109/JPROC.2002.1021562.
7. Li Y, Zhao M, Deng Y, Tian D, Ma X. Research on dispatching for wind power integrated system based on wind turbine fatigue character. International Conference on Renewable Power Generation (RPG 2015), Beijing. 2015;1-6. DOI: 10.1049/cp.2015.0434.
8. Rashid MH. Power Electronics Handbook. San Diego, CA: Academic Press; 2007. Available:http://site.iugaza.edu.ps/malramlawi/files/RASHID_Power_Electronics_Handbook/ pdf.
9. Salman A, Williams A, Amjad H, Bhatti MKL, Saad M. Simplified modeling of a PV panel by using PSIM and its comparison with laboratory test results. Proceedings of the 5th IEEE Global Humanitarian Technology Conference, Seattle, Washington, USA; 2015.

DOI:10.13140/RG.2.2.15106.07367.
10. Shea JJ. Clean electricity from photovoltaics. IEEE Electrical Insulation Magazine. 2002;18(4):46-47.
DOI: 10.1109/MEI.2002.1019908.
11. Villalva M, Gazoli J, Filho E. Comprehensive approach to modeling and simulation of photovoltaic arrays. IEEE Transactions on Power Electronics. 2009;24(5):1198-1208.
DOI:10.1109/TPEL.2009.2013862.
12. Li W, Zhao Y, Deng Y, He X. Interleaved converter with voltage multiplier cell for high step-up and high-efficiency conversion. IEEE Transactions on Power Electronics. 2019;25(9):2397–2408.
DOI:10.1109/TPEL.2010.2048340.
13. Hussein HI. On-Line UPS with low frequency transformer for isolation. Iraq Journal of Electrical and Electronic Engineering. 2014;10(2):100-106.
DOI: 10.37917/ijeee.10.2.5.
14. Ehikhamenle M, Okeke RO. Design and development of 2.5KVA inverter adopting a microcontroller based frequency meter. International Journal of Engineering and Modern Technology. 2017;3(1):1-14.
15. Diouri O, Es-Sbai N, Errahimi F, Gaga A, Alaoui C. Modeling and design of single phase pv inverter with MPPT algorithm applied to the boost converter using back stepping control in standalone mode. Hindawi International Journal of Photo-energy. 2019;1(1):1-16.
DOI:doi.org/10.1155/2019/7021578.
16. Suresh P, Gopi K, Shaik RK. Transformerless inverter for grid-connected photovoltaic systems using fuzzy logic controller. International Journal of Advanced Engineering Research and Science (IJAERS) Trends in Engineering and Technology (NCTET-2K17). 2017;1(5):149-156.
DOI:doi.org/10.22161/ijaers/nctet.2017.eee.51.
17. Muhanned A. Solar energy conversion using low cost inverter. Land Forces Academy Review. 2019;24(2):151-157.
DOI: 10.2478/raft-2019-0018.
18. Khan MT, Milani AA, Chakrabortty A, Husain I. Dynamic modeling and feasibility analysis of a solid-state transformer-based power distribution system. IEEE Transactions on Industry Applications. 2017 Sep 27;54(1):551-62.
DOI: 10.1109/TIA.2017.2757450.
19. Khan UA, Ali Khan A, Akbar F, Park JW. A novel high-frequency isolated single-phase full-bridge buck-boost inverter. IECON 2021 – 47th Annual Conference of the IEEE Industrial Electronics Society. 2021:1-6.
DOI: 10.1109/IECON48115.2021.9589949.
20. Patel HD, Patel ND, Patel AN, Soni RR. Design and development of high frequency transformer for isolated DC-DC converter. In 2012 1st International Conference on Emerging Technology Trends in Electronics, Communication & Networking. 2012;1-4.
DOI: 10.1109/ET2ECN.2012.6470074.
21. Jiang S, Cao D, Peng FZ. High frequency transformer isolated Z-source inverters. In 2011 Twenty-Sixth Annual IEEE Applied Power Electronics Conference and Exposition (APEC). 2011;442-449.
DOI: 10.1109/APEC.2011.5744634.
22. Kjaer SB, Pedersen JK, Blaabjerg F. A review of single-phase grid-connected inverters for photovoltaic modules. IEEE Transactions on Industry Applications. 2005;41(5):1292–1306.
DOI:10.1109/TIA.2005.853371.
23. Yang LS, Liang TJ, Chen JF. Transformerless DC-DC converters with high step up voltage gain. IEEE Trans. Ind. Electron. 2009;56(8):3144–3152.
DOI:10.1109/TIE.2009.2022512.
24. Xue Y, Chang L, Kjær SB, Bordonau J, Shimizu T. Topologies of single-phase inverters for small distributed power generators: An overview. IEEE Transactions on Power Electronics. 2004;19(5):1305-1314.
DOI: 10.1109/TPEL.2004.833460.
25. Deepa R, Nagashree AN, Anand K. Transformerless grid connected single phase inverter for power system application. In 2015 International Conference on Emerging Research in Electronics, Computer Science and Technology (ICERECT). 2015:418-422.
DOI: 10.1109/ERECT.2015.7499052.
26. Kolantla D, Mikkili S, Pendem SR, Desai AA. Critical review on various inverter topologies for PV system architectures. IET Renewable Power Generation. 2020;14(17):3418-3438.
DOI: 10.1049/iet-rpg.2020.0317.
27. Taghvaie A, Haque ME, Saha S, Mahmud MA. A multilevel solid-state transformer-based grid-connected solar photovoltaic systems. In 2021 IEEE Industry

Applications Society Annual Meeting (IAS). 2021 Oct 10;1-7. IEEE. DOI:10.1109/IAS48185.2021.9677143.
28. Rashid MH. (Ed.). Power electronics handbook. 3rd ed. Oxford, United Kingdom: Butterworth-Heinemann; 2011.
29. Eichhorn T. Boost converter efficiency through accurate calculations. Power Electronics Technology; 2008. Accessed 16 September 2021. Available:https://www.researchgate.net/publication/291489548
30. Fedkin M. Efficiency of inverters (EME 812 online open courseware: utility solar power and concentration); 2020. Accessed 27 September 2021. Available:https://www.e-education.psu.edu/eme812/node/738.
31. Guo X, Wang N, Jianhua Z, Baocheng W, Minh-Khai N. A Novel Transformerless Current Source Inverter for Leakage Current Reduction. IEEE ACCESS. 2019;7(2019):50681-50690. DOI: 10.1109/ACCESS.2019.2908287.
32. Kerekes T, Teodorescu R, Rodríguez P, Vázquez G, Aldabas E. A new high efficiency single-phase transformerless PV inverter topology. IEEE Transactions on Industrial Electronics. 2009;58(1):184–191. DOI: 10.1109/TIE.2009.2024092.
33. Chakraborty S, Razzak MA. Design of a transformer-less grid-tie inverter using dual-stage buck and boost converters. International Journal of Renewable Energy Research. 2014;4(1):91-98.
34. Umesh AK, Shamkumar BC, Mahesh SC. Design and simulation of transformer less single phase photovoltaic inverter without battery for domestic application. IOSR Journal of Electrical and Electronics Engineering (IOSR-JEEE). 2015;10(1):88-93.
35. Babarinde OO, Adeleke BS, Adeyeye AH, Ogundeji OA, Ganiyu AL. Design and construction of 1kVA inverter. International Journal of Emerging Engineering Research and Technology (IJEERT). 2014;2(3):201-212.

Peer-review history:
The peer review history for this paper can be accessed here:
https://www.sdiarticle5.com/review-history/91935